

RARE DECAYS AT LHCb*

I. BELYAEV

On behalf of LHCb Collaboration

Department of Physics, Syracuse University, Syracuse, NY 13244, USA

(Received November 15, 2006)

Rare loop-induced decays are sensitive to New Physics in many Standard Model extensions. In this paper we discuss the reconstruction of the radiative penguin decays $B_d^0 \rightarrow K^{*0}\gamma$, $B_s^0 \rightarrow \phi\gamma$, $B_d^0 \rightarrow \omega\gamma$, $\Lambda_b \rightarrow \Lambda\gamma$, the electroweak penguin decays $B_d^0 \rightarrow K^{*0}\mu^+\mu^-$, $B_u^+ \rightarrow K^+\mu^+\mu^-$, the gluonic penguin decays $B_d^0 \rightarrow \phi K_S^0$, $B_s^0 \rightarrow \phi\phi$ and the decay $B_s^0 \rightarrow \mu^+\mu^-$ at LHCb. The selection criteria, evaluated efficiencies, expected annual yields and B/S estimates are presented.

PACS numbers: 14.40.Nd, 12.60.-i

1. Introduction

Studies of the rare radiative penguin decays $B_d^0 \rightarrow K^{*0}\gamma$, $B_s^0 \rightarrow \phi\gamma$, $B_d^0 \rightarrow \omega\gamma$, $\Lambda_b \rightarrow \Lambda\gamma$, the electroweak penguin decays $B_d^0 \rightarrow K^{*0}\mu^+\mu^-$, $B_u^+ \rightarrow K^+\mu^+\mu^-$, the gluonic penguin decays $B_d^0 \rightarrow \phi K_S^0$, $B_s^0 \rightarrow \phi\phi$ and the decay $B_s^0 \rightarrow \mu^+\mu^-$ allow to extract valuable information about penguin and box loop-diagrams (see Fig. 1).

Such diagrams are suppressed in the Standard Model (SM) due to GIM cancellation of different quark contributions. This cancellation is perfect in the limit of equal quark masses due to unitarity of the CKM-matrix. New particles arising in SM extensions in general do not preserve this cancellation and manifest themselves in particular in enhancements of loop amplitudes. For example the $B_s^0 \rightarrow \mu^+\mu^-$ rate, predicted to be 3.5×10^{-9} in the SM [1], is enhanced by a factor $\tan^6 \beta$ in SUSY models [2].

The complex couplings of new particles may result in the appearance of non-trivial CP-violating phases, disturbing the CP-asymmetries predicted by the SM. For example for the decay $B_d^0 \rightarrow K^{*0}\gamma$ due to one-diagram dominance (the strong phase appears only at order α_S and $1/m_b$) the direct

* Presented at the "Physics at LHC" Conference, Kraków, Poland, July 3–8, 2006.

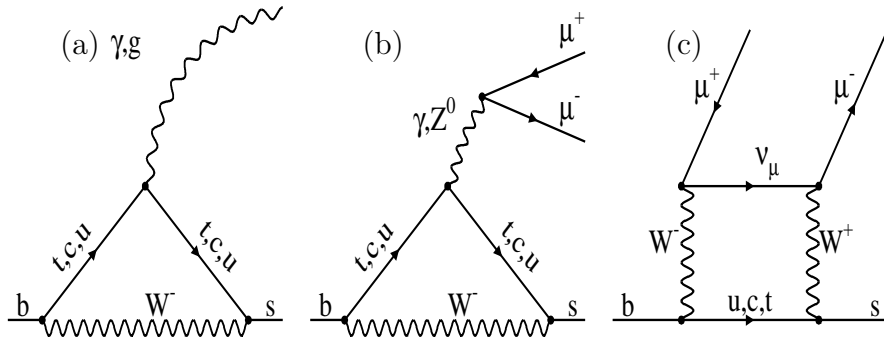


Fig. 1. Loop diagrams which make the major contributions to $B_d^0 \rightarrow K^{*0}\gamma$, $B_s^0 \rightarrow \phi\gamma$, $B_d^0 \rightarrow \omega\gamma$, $\Lambda_b \rightarrow \Lambda\gamma$ (diagram (a) with a virtual photon), $B_d^0 \rightarrow \phi K_S^0$, $B_s^0 \rightarrow \phi\phi$ (diagram (a) with a virtual gluon), $B_d^0 \rightarrow K^{*0}\mu^+\mu^-$, $B_u^+ \rightarrow K^+\mu^+\mu^-$ (diagrams (b) and (c)), $B_s^0 \rightarrow \mu^+\mu^-$ (diagram (c)) decays.

CP-asymmetry is reliably predicted in the SM to be $\leq 1\%$ [3], but for some SUSY scenarios it could be as large as 10–40% [3, 4].

Due to the $V-A$ structure of the weak current the photon polarization in $b \rightarrow s(d)\gamma$ transitions is almost 100%. However, QCD corrections increase the fraction of wrongly polarized photons up to $O(10\%)$ [5]. The smallness of this quantity in the SM causes the mixing-induced CP-asymmetries to vanish [6], while in extensions of the SM these asymmetries could be as large as 50% [7]. This effect can be used as a probe for the spin structure of new particles.

Radiative decays of polarized beauty baryons like $\Lambda_b \rightarrow \Lambda\gamma$ can be used to probe the chirality of the effective Hamiltonian by measuring the photon polarization [8]. The angular asymmetry between the Λ_b spin and the photon momentum combined with the $\Lambda^0 \rightarrow p\pi$ decay polarization probes the predicted $V-A$ structure of this decay.

The forward–backward asymmetry $A_{FB}(q^2)$ for the decay $B_d^0 \rightarrow K^{*0}\mu^+\mu^-$, is defined through the angle θ_{FB} between the μ^+ and K^{*0} momenta in the dimuon rest frame¹. The shape of the asymmetry $A_{FB}(q^2)$ and especially the position of the zero crossing in the SM are almost unaffected by hadronic form factor uncertainties, thus providing a good basis for searching for deviations [9].

The ratio of $b \rightarrow s\mu^+\mu^-$ and $b \rightarrow se^+e^-$ decays in any exclusive mode, e.g. $B_u^+ \rightarrow K^+\ell^+\ell^-$, is also a clean probe of the SM. Lepton-universality predicts this ratio to be 1 with theoretical errors below 1% [10].

¹ q^2 is the dimuon invariant mass squared.

The tiny hint for possible discrepancy between the measured mixing-induced CP asymmetries in gluonic $b \rightarrow s$ transitions and the world average for the parameter $\sin 2\beta$ measured in charmonium modes [11] points to the necessity and importance for careful and intensive studies of gluonic penguin dominated decays.

The test of QCD models in radiative penguin decays still plays an important role [12]. The ratio $|V_{td}|/|V_{ts}|$ could be extracted from $\Gamma(B_d^0 \rightarrow \omega\gamma)/\Gamma(B_d^0 \rightarrow K^{*0}\gamma)$ with moderate theoretical uncertainty.

2. Reconstruction of B -decays at LHCb

LHCb is a forward spectrometer at LHC. The detector is described elsewhere [13–15]. The reconstruction of rare B -decays at LHCb is a challenge due to the small rates and large backgrounds from various sources. The most critical background is combinatorial background from $pp \rightarrow b\bar{b}X$ events, containing primary and secondary vertices and characterized by high charged and neutral multiplicities. We studied the forward $pp \rightarrow b\bar{b}X$ production as the dominating background, where at least one b -hadron is emitted forward within 400 mrad of the beam axis.

The studies have been performed using fully simulated events [15]. The detailed description of the charged particle identification in LHCb, based on a combined analysis of information from Čerenkov Detectors, Muon and Calorimeter Systems can be found elsewhere [15–19]. Photon candidates have been defined as clusters in the electromagnetic calorimeter not associated with any charged track [15, 18–20]. The reconstruction of π^0 and K_S^0 is described in [15, 20, 21].

The background suppression exploits the generic properties of beauty production at pp -collisions. The large mass of beauty hadrons results in hard transverse momentum spectra of secondary particles. The large lifetime, $\langle\beta\gamma c\tau\rangle \sim 5$ mm, results in a good isolation of the B decay vertex and the inconsistency of B -decay products with the reconstructed pp -collision vertex.

For events with several reconstructed primary vertices the primary vertex with the minimum B -candidate impact parameter has been chosen as the B production vertex [15].

The background from minimum bias events can be significant, but it has been assumed that this contribution is drastically suppressed at the trigger level, which exploits the hard transverse momentum spectra of b -decay products and large impact parameters of tracks from b -decays with respect to primary vertices [22].

To cope with the limited available Monte Carlo statistics, the B mass cut has been relaxed when analyzing these events. The background under the B mass peak has been estimated in the enlarged mass interval assuming

a linear dependence on the reconstructed B_d^0 (B_s^0) mass (after removal of events with a true signal decay or similar decays which necessarily lead to a reconstructed mass outside the tight mass window). In addition, in order to further increase the effective $pp \rightarrow b\bar{b}X$ statistics, all B/S ratios have been estimated without applying the trigger criteria.

In the evaluation of trigger efficiencies, a 100% efficiency for the High Level Triggers has been assumed. Other assumptions, parameters and branching ratios used for the evaluation of signal yields can be found elsewhere [15, 23–34].

2.1. Radiative penguin decays

For the reconstruction of $B_d^0 \rightarrow K^{*0}\gamma$ and $B_s^0 \rightarrow \phi\gamma$ decays [15, 23–27] K^{*0} and ϕ candidates have been reconstructed in the $K^+\pi^-$ and K^+K^- modes, respectively².

Identified charged tracks have to be inconsistent with any reconstructed primary vertex. This requirement is especially effective to suppress combinatoric background for events with multiple pp -interactions [23]. A vertex fit has been applied to two tracks forming K^{*0} (ϕ) candidates. The mass window of $K^+\pi^-$ (K^+K^-) combinations has been chosen to be ± 60 (10) MeV/c^2 around the nominal K^{*0} (ϕ) mass³.

Selected K^{*0} (ϕ) candidates have been combined with photon candidates. The requirement on the transverse energy of the photon candidate to be greater than 2.8 GeV efficiently removes low energy γ and π^0 . The transverse energy of the photon candidate with respect to the B_d^0 (B_s^0) candidate flight direction has to be within the interval 2.2 (2.0)–2.7 GeV.

The K^{*0} (ϕ) decay vertex has been considered as the B_d^0 (B_s^0)-decay vertex. The angle θ_B between the momentum vector of the reconstructed B_d^0 (B_s^0) candidate and the flight path vector from the B_d^0 (B_s^0) production to the B_d^0 (B_s^0) decay vertex is required to be smaller than 6(15) mrad. This requirement is one of the most powerful cuts against combinatorial background as demonstrated in Fig. 2. The smaller opening angle between the two kaons results in a larger uncertainty in the position of the secondary vertex and, therefore, degraded resolution in θ_B .

Background from the decays $B_d^0 \rightarrow K^{*0}\pi^0$ and $B_s^0 \rightarrow \phi\pi^0$ with an energetic π^0 reconstructed as a single photon has been suppressed by requiring that $|\cos\theta| < 0.7$, where θ is the helicity angle between the B and the K^+ in the K^{*0} (ϕ) rest frame. The invariant mass distributions of the selected and triggered $B_d^0 \rightarrow K^{*0}\gamma$ and $B_s^0 \rightarrow \phi\gamma$ candidates are shown in Figs. 3(a) and 3(b). In both cases the mass resolution has been found to be $\sim 65 \text{ MeV}/c^2$.

² The charge conjugate mode is always implied unless explicitly stated otherwise.

³ The cut values given in parentheses have been applied to the $B_s^0 \rightarrow \phi\gamma$ selection.

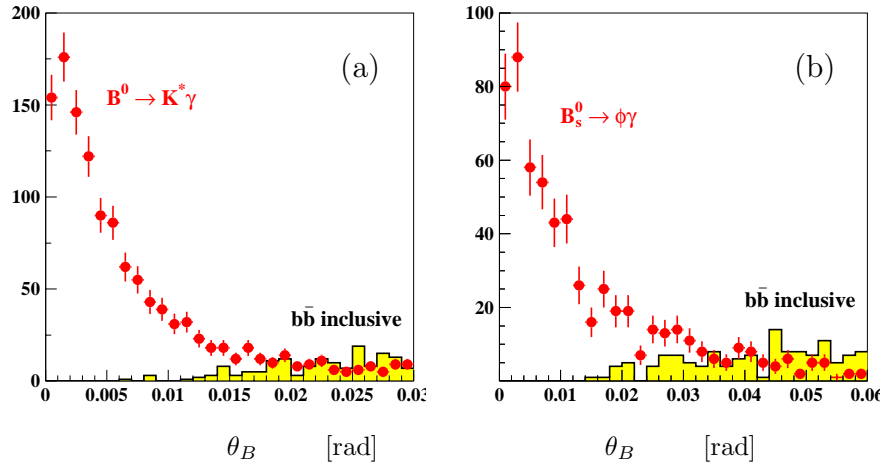


Fig. 2. Distributions of the angle θ_B for signal events (points with error bars) and forward $pp \rightarrow b\bar{b}X$ events (filled histogram): (a) $B_d^0 \rightarrow K^* \gamma$, (b) $B_s^0 \rightarrow \phi \gamma$.

The selection of the decay $B_d^0 \rightarrow \omega \gamma$ followed by $\omega \rightarrow \pi^+ \pi^- \pi^0$ follows a similar approach, but it is complicated by the π^0 reconstruction [20]. The invariant mass distribution for the selected and triggered $B_d^0 \rightarrow \omega \gamma$ candidates is shown in Fig. 3(c).

The same selection ideas have been applied to the reconstruction of radiative decays of Λ_b baryon to $\Lambda \gamma$. While the reconstruction of the final states with the heavy Λ resonances decaying strongly to pK is very similar to reconstruction of final states with K^{*0} and ϕ , the reconstruction of $\Lambda^0 \gamma$

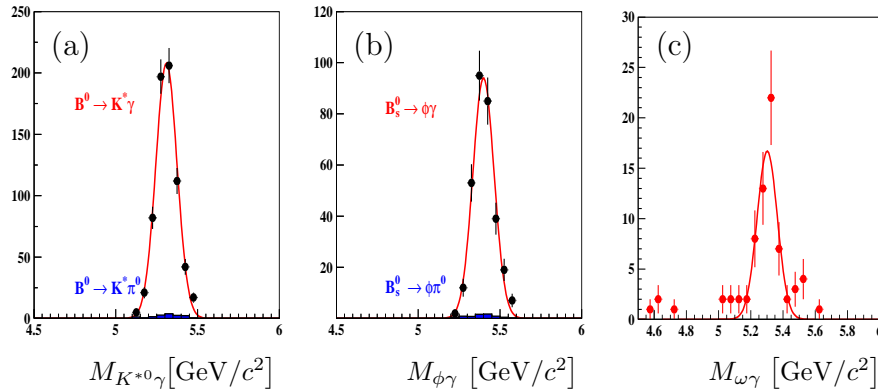


Fig. 3. Invariant mass distributions for signal events after trigger and selection cuts: (a) $B_d^0 \rightarrow K^{*0} \gamma$, (b) $B_s^0 \rightarrow \phi \gamma$, (c) $B_d^0 \rightarrow \omega \gamma$. The absolute normalization is arbitrary. The specific background from $B_d^0 \rightarrow K^{*0} \pi^0$ and $B_s^0 \rightarrow \phi \pi^0$ decays is shown in on (a) and (b) with proper normalization.

is a bit more delicate since at the LHC A^0 may traverse a large fraction of the tracking system before decaying [28, 35].

Due to the dedicated trigger for energetic photons, the high trigger efficiency for selected events of 35 % [15, 22] is achieved for all radiative channels.

2.2. Electroweak penguin decays $B_d^0 \rightarrow K^{*0} \mu^+ \mu^-$ and $B_u^+ \rightarrow K^+ \mu^+ \mu^-$

Dimuon candidates have been selected [29, 30] from muons with a transverse momentum in excess of 900 MeV/c, originating from a common vertex. Dimuon candidates with an invariant mass in the mass intervals populated by $J/\psi \rightarrow \mu^+ \mu^-$ and $\psi(2S) \rightarrow \mu^+ \mu^-$ decays⁴ have been excluded from the analysis.

$K^+ \pi^-$ combinations with an invariant mass in the interval of ± 0.1 GeV/ c^2 around the nominal K^{*0} mass and originating from common vertex have been considered as K^{*0} candidates. The transverse momentum of pions from K^{*0} candidates has been required to be larger than 200 MeV/ c^2 .

A vertex fit has been applied for pairs of selected dimuon and K^{*0} candidates. The significance of the B_d^0 impact parameter with respect to its production vertex has been required to be small, while a lower cut has been applied on the significance of the distance between the production vertex and the B_d^0 -decay vertex. Kaons and pions from the K^{*0} are required to be inconsistent with the B_d^0 -production vertex. In addition a cut has been applied on the maximum multiplicity of tracks consistent with the B_d^0 -decay vertex. This requirement improves the isolation of the B_d^0 decay vertex.

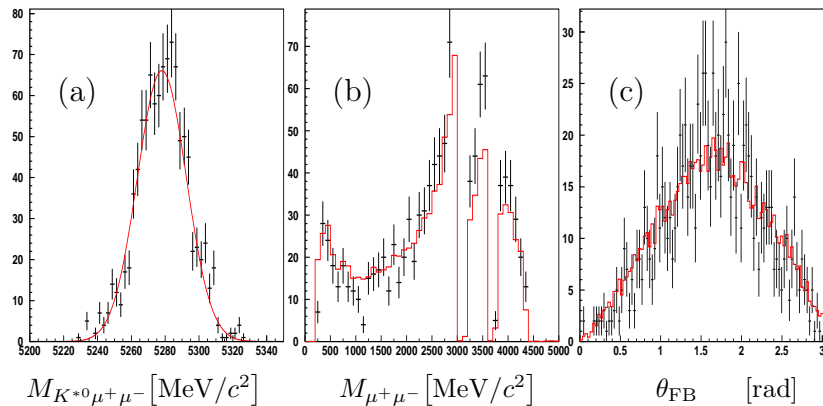


Fig. 4. (a) The $K^{*0} \mu^+ \mu^-$ invariant mass distribution for $B_u^+ \rightarrow K^+ \mu^+ \mu^-$ events. The distributions of $\mu^+ \mu^-$ invariant mass (b) and angle θ_{FB} (c) for $B_u^+ \rightarrow K^+ \mu^+ \mu^-$ events (points with error bars), superimposed with the scaled distributions at generator level (solid histogram).

⁴ The excluded intervals have been defined as 2.9–3.2 and 3.65–3.75 GeV/ c^2 .

The invariant mass distribution for signal events after selection cuts is shown in Fig. 4(a). The B_d^0 mass resolution has been found to be $15 \text{ MeV}/c^2$. The distributions for the dimuon invariant mass and the angle θ_{FB} are not distorted by acceptance or selection cuts, as illustrated in Figs. 4(b) and 4(c). The resolution on these observables has been estimated to be $9.7 \text{ MeV}/c^2$ and 4 mrad , respectively.

For the measurement of the ratio of partial width $\Gamma(B_u^+ \rightarrow Ke^+e^-)$ and $\Gamma(B_u^+ \rightarrow K\mu^+\mu^-)$ the dilepton mass range has been chosen to be $1 < m_{\ell\ell}^2 < 6 \text{ GeV}^2/c^4$ in order to avoid $c\bar{c}$ resonances (especially in e^+e^- mode) and threshold effects due to higher muon mass. The decays $B_u^+ \rightarrow Ke^+e^-$ and $B_u^+ \rightarrow K\mu^+\mu^-$ has been reconstructed using the similar criteria. A proper bremsstrahlung correction [15,19] is essential for channel with electrons. The expected mass distributions are shown in Fig. 5.

It is worth to mention that the final state with a dimuon candidate has a trigger efficiency of 74 % for selected events [29].

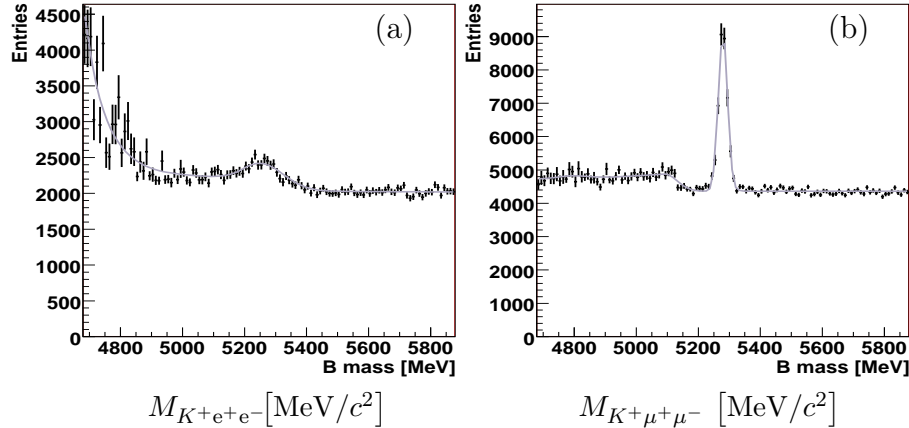


Fig. 5. The $K^+\ell^+\ell^-$ invariant mass distributions: (a) $K^+e^+e^-$ and (b) $K^+\mu^+\mu^-$.

2.3. Gluonic penguin decays $B_s^0 \rightarrow \phi\phi$ and $B_d^0 \rightarrow \phi K_S^0$

Kaons inconsistent with any reconstructed primary vertex in the event have been used for the reconstruction of ϕ candidates [31–33]. A vertex fit has been applied to K^+K^- pairs and a mass window of $\pm 12(17) \text{ MeV}/c^2$ around the nominal ϕ mass has been chosen⁵.

K_S^0 candidates have been reconstructed as a $\pi^+\pi^-$ pair originating from a common secondary vertex. Three different categories of charged tracks have been used for the K_S^0 reconstruction: it long (tracks with hits both in the vertex detector before the magnet and the main tracker system after

⁵ The cut values given in parentheses has been applied to the $B_d^0 \rightarrow \phi K_S^0$ selection.

the magnet), *downstream* (tracks with no hits in the vertex detector) and *upstream* (tracks with no hits in the main tracker system) [15,21]. The mass window has been defined to be $\pm 25 \text{ MeV}/c^2$ for pairs of two *downstream* tracks and $\pm 15 \text{ MeV}/c^2$ for all other combinations [21, 32, 33]. The transverse momentum of K_S^0 candidates has been required to be greater than $1.1 \text{ GeV}/c$ for K_S^0 candidates from pairs of *downstream* tracks and greater than $500 \text{ MeV}/c$ for all other combinations.

Pairs of selected ϕ from a common vertex have been considered as B_s^0 candidates if the decay angle θ between the ϕ momentum in the rest frame of the $\phi\phi$ system and the direction of the Lorentz boost from the laboratory frame to the $\phi\phi$ rest frame satisfies $|\cos\theta| < 0.75$. Pairs of selected ϕ and K_S^0 have been considered as B_d^0 candidates if they originate from a common vertex and the transverse momentum of the ϕ exceeds $1.35 \text{ GeV}/c^2$. A cut on the minimal impact parameter of the ϕK_S^0 pair with respect to all primary vertices has been used to suppress further the background. The value of this cut has been chosen to be $250 \mu\text{m}$, $200 \mu\text{m}$ and $100 \mu\text{m}$ for K_S^0 candidates reconstructed from *downstream-downstream*, *long-long* pairs and other combinations correspondingly. The opening angle between the momentum of the B_s^0 (B_d^0) candidate and the flight path vector has been required to be smaller than $10(15) \text{ mrad}$. The cut can be tighter in the case of $B_s^0 \rightarrow \phi\phi$ decay since the 4-prong $\phi\phi$ vertex gives a better vertex resolution.

The invariant mass distributions of the selected and triggered $B_s^0 \rightarrow \phi\phi$ and $B_d^0 \rightarrow \phi K_S^0$ candidates are shown in Figs. 6(a) and 6(b). The mass resolutions for B_s^0 and B_d^0 decays have been found to be $12 \text{ MeV}/c^2$ and $16 \text{ MeV}/c^2$, respectively.

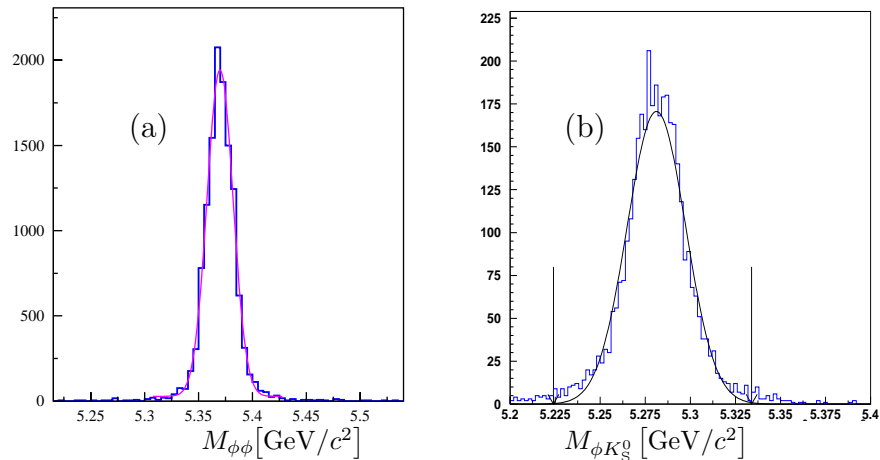


Fig. 6. The invariant mass of B_s^0 (B_d^0) candidates after selection and trigger cuts: (a) $B_s^0 \rightarrow \phi\phi$, (b) $B_d^0 \rightarrow \phi K_S^0$.

2.4. Decay $B_s^0 \rightarrow \mu^+ \mu^-$

Since two-body B_s^0 -decays are characterized by high transverse momenta of the decay products, only muons with a transverse momentum in excess of $1.5 \text{ GeV}/c$ have been selected for the $B_s^0 \rightarrow \mu^+ \mu^-$ reconstruction [34]. A vertex fit has been applied for dimuon combinations. The transverse momentum of muon pairs has been required to exceed $3.5 \text{ GeV}/c^2$. Dimuons with a small impact parameter with respect to the chosen primary vertex have been considered as B_s^0 candidates.

For selected B_s^0 candidates the separation between the reconstructed dimuon vertex and the primary vertex has been required to be large.

The dimuon invariant mass resolution has been found to be $18 \text{ MeV}/c^2$. The trigger efficiency for events that passed the selection criteria has been found to be 79 %.

2.5. Signal yields and background-to-signal ratios

The expected signal event yields for 2 fb^{-1} accumulated luminosity together with estimates for background-to-signal ratios (B/S) are presented in Table I.

TABLE I

The expected event yields for 2 fb^{-1} accumulated luminosity for rare B -decays and the estimates for background-to-signal ratios (B/S). The cited upper limits are at 90% CL.

Channel	Yield/ 2 fb^{-1}	B/S
$B_d^0 \rightarrow K^{*0} \gamma$	3.5×10^4	< 0.7
$B_s^0 \rightarrow \phi \gamma$	9.3×10^3	< 2.4
$B_d^0 \rightarrow \omega \gamma$	40	< 3.5
$\Lambda_b \rightarrow \Lambda^0 \gamma$	750	< 42
$\Lambda_b \rightarrow \Lambda(1520) \gamma$	4.2×10^3	< 10
$\Lambda_b \rightarrow \Lambda(1670) \gamma$	2.5×10^3	< 18
$\Lambda_b \rightarrow \Lambda(1520) \gamma$	2.5×10^3	< 18
$B_d^0 \rightarrow K^{*0} \mu^+ \mu^-$	4.4×10^3	< 2.0
$B_u^+ \rightarrow K e^+ e^-$	350	~ 5
$B_u^+ \rightarrow K \mu^+ \mu^-$	1.6×10^3	~ 3
$B_d^0 \rightarrow \phi K_S^0$	800	< 1.1
$B_s^0 \rightarrow \phi \phi$	1.2×10^3	< 0.2
$B_s^0 \rightarrow \mu^+ \mu^-$	17	< 440

As mentioned in Sec. 2, the forward $pp \rightarrow b\bar{b}X$ production is considered as the dominant background.

The relative contribution of the correlated background from $B_d^0 \rightarrow K^{*0}\pi^0$ and $B_s^0 \rightarrow \phi\pi^0$ decays to the radiative penguin decays $B_d^0 \rightarrow K^{*0}\gamma$ and $B_s^0 \rightarrow \phi\gamma$ has been estimated to be small ($B_{K^{*0}\pi^0}/S < 2.2\%$ for $B_d^0 \rightarrow K^{*0}\gamma$ and $B_{\phi\pi^0}/S < 4.0\%$ for $B_s^0 \rightarrow \phi\gamma$) [23, 25].

The relative background contribution from inclusive ϕ production in b -decays to selected $B_d^0 \rightarrow \phi K_S^0$ events has been estimated to be $B_b \rightarrow \phi/S < 0.28$. A sample of 10^6 fully simulated $pp \rightarrow (b \rightarrow \phi X) X$ events has been analyzed [32, 33].

For the $B_u^+ \rightarrow K^+\mu^+\mu^-$ analysis, events with dimuons have been studied as potential background. Samples of 10^7 fully simulated $pp \rightarrow (b \rightarrow \mu X) (\bar{b} \rightarrow \mu X) X$ and 2×10^5 $pp \rightarrow (b \rightarrow \mu^- (c \rightarrow \mu^+ X) X) X$ events have been used. The contribution of the background with two muons from semileptonic $b \rightarrow \mu\nu_\mu X$ -decays has been evaluated to be $B_{\mu\mu}/S = 0.5 \pm 0.2$. The contribution of the background with one primary and one cascade muon has been evaluated to be $B_{\mu\mu'}/S < 1.1$. Contributions from the exclusive decays $B_d^0 \rightarrow J/\psi K^{*0}$, $B_d^0 \rightarrow J/\psi K_S^0$ and $B_s^0 \rightarrow J/\psi\phi$ have been found to be smaller than 5% each [29, 30].

The feed-down to selected $B_s^0 \rightarrow \mu^+\mu^-$ events from exclusive two-prong decays of b -hadrons with misidentified muons has been evaluated to be an order of magnitude smaller than the signal yield in a ± 25 MeV/ c^2 window around the nominal B_s^0 mass [36, 37]. The background contribution from $pp \rightarrow (b \rightarrow \mu X) (\bar{b} \rightarrow \mu X) X$ events has been evaluated to be $B_{\mu\mu}/S < 5.7$ [34].

3. Conclusion

The LHCb experiment has promising physics potential for the study of numerous loop-induced rare decays such as the radiative penguin decays $B_d^0 \rightarrow K^{*0}\gamma$, $B_s^0 \rightarrow \phi\gamma$, $B_d^0 \rightarrow \omega\gamma$, $\Lambda_b \rightarrow \Lambda\gamma$ the electroweak penguin decays $B_d^0 \rightarrow K^{*0}\mu^+\mu^-$, $B_u^+ \rightarrow Ke^+e^-$, and $B_u^+ \rightarrow K\mu^+\mu^-$, the gluonic penguin decays $B_s^0 \rightarrow \phi\phi$ and $B_d^0 \rightarrow \phi K_S^0$ and the rare box decay $B_s^0 \rightarrow \mu^+\mu^-$. The expected signal event yields for 2fb^{-1} and preliminary estimates on background-to-signal ratios have been presented.

These yields (2fb^{-1}) will allow to measure the direct CP-asymmetry for $B_d^0 \rightarrow K^{*0}\gamma$ decays with statistical uncertainty well below 1%. The expected statistical error on the ratio $|V_{td}|/|V_{ts}|$ extracted from $\Gamma(B_d^0 \rightarrow \omega\gamma)/\Gamma(B_d^0 \rightarrow K^{*0}\gamma)$ is $O(10\%\sqrt{1+B/S})$.

For five years of data taking (10fb^{-1}) the expected precision of the fraction of right-handed photons from decays $\Lambda_b \rightarrow \Lambda\gamma$ is 5% and the precision on the position of zero crossing for $A_{\text{FB}}(q^2)$ is $0.5\text{GeV}^2/c^4$. The error on the ratio of integrated partial width $B_u^+ \rightarrow Ke^+e^-$ and $B_u^+ \rightarrow K\mu^+\mu^-$ is expected to be 4%.

The precision and reliability of background-to-signal estimations are expected to improve with a significant increase of Monte Carlo samples. Studies of high level trigger efficiencies, systematic uncertainties, and the sensitivity to new physics, as well as studies of other interesting rare decays, *e.g.* $B_d^0 \rightarrow \rho^0 \gamma$, $B_s^0 \rightarrow \phi \ell^+ \ell^-$ *etc.*, are in progress.

It is a great pleasure to thank the Drs. G. Pakhlova, S. Barsuk and P. Koppenburg for extremely pleasant cooperation, Drs. S. Amato, F. Legger, O. Leroy, J.H. Lopes, F. Marinho, B. de Paula, B. Viaud, Y. Xie and Profs. E. Aslanides, R. Le Gac, A. Tsaregorodtsev for their leading contributions to this work, Dr. G. Raven and Profs. A. Golutvin, U. Egede and T. Nakada for useful discussions.

REFERENCES

- [1] A. Ali, [hep/ph-9702312](#).
- [2] G. Buchalla, A.J. Buras, *Nucl. Phys.* **B398**, 285 (1993); G. Buchalla, A.J. Buras, *Nucl. Phys.* **B400**, 225 (1993); G. Buchalla, A.J. Buras, CERN-TH-1998-369.
- [3] T. Hurth, T. Mannel, CERN-TH-2001-242.
- [4] M. Neubert, CLNS-03-1814.
- [5] B. Grinstein, Y. Grossman, Z. Ligeti, D. Pirjol, *Phys. Rev.* **D71**, 011504 (2005).
- [6] M. Gronau, EFI-03-17.
- [7] D. Atwood, M. Gronau, A. Soni, *Phys. Rev. Lett.* **79**, 185 (1997); A. Masiero, TUM-HEP-303-97.
- [8] T. Mannel, S. Recksiegel, *Nucl. Part. Phys.* **24**, 979 (1998).
- [9] A. Ali, [hep-ph/0210183](#).
- [10] G. Hiller, F. Krüger, *Phys. Rev.* **D69**, 074020 (2004).
- [11] S. Eidelman *et al.*, *Phys. Lett.* **B592**, 1 (2004).
- [12] M. Neubert, [hep-ph/0110301](#).
- [13] H. Dijkstra *et al.*, LHCb-95-001.
- [14] S. Amato *et al.*, CERN-LHCC-98-004.
- [15] R. Antunes Nobrega *et al.*, CERN-LHCC-2003-030.
- [16] S. Amato *et al.*, CERN-LHCC-2000-037.
- [17] P.R. Barbosa Marinho *et al.*, CERN-LHCC-2001-010; P.R. Barbosa Marinho *et al.*, CERN-LHCC-2003-003.
- [18] S. Amato *et al.*, CERN-LHCC-2000-036.
- [19] H. Terrier, I. Belyaev, LHCb-2003-092.

- [20] O. Deschamps *et al.*, LHCb-2003-091.
- [21] LHCb-2003-088.
- [22] R. Antunes Nobrega *et al.*, CERN-LHCC-2003-031.
- [23] G. Pakhlova, I. Belyaev, LHCb-2003-090.
- [24] I. Belyaev, Ph.D. theses, ITEP/Moscow, 2005.
- [25] G. Pakhlova, *Czech. J. Phys. Suppl. A* **54**, (2004).
- [26] I. Belyaev, *Czech. J. Phys.* **55**, B485 (2005).
- [27] S. Barsuk, G. Pakhlova, I. Belyaev, *Phys. At. Nucl.* **69**, 623 (2006).
- [28] F. Legger, Ph.D. Theses, EPFL, 2006.
- [29] J.H. Lopes, LHCb-2003-104.
- [30] J.H. Lopes, *Czech. J. Phys. Suppl. A* **54**, (2004).
- [31] S. Barsuk, I. Belyaev, LHCb-2003-094.
- [32] E. Aslanides *et al.*, LHCb-2004-001.
- [33] B. Viaud, Ph.D. theses, CPPM-T-2003-06.
- [34] B. de Paula, F. Marinho, S. Amato, LHCb-2003-16.
- [35] F. Legger, T. Schietinger, [hep-ph/0605245](#).
- [36] E. Polycarpo, LHCb-2002-027.
- [37] E. Polycarpo, Ph.D. thesis, CERN-THESIS-2002-023.